Machine learning for predicting DataCube atomic force microscope (AFM)-MultiDAT-AFM

Germanicus Rosine, El-Hassani Othman

ISTFA 2024: Proceedings from the 50th International Symposium for Testing and Failure Analysis Conference
October 28–November 1, 2024, San Diego, California, USA
https://doi.org/10.31399/asm.cp.istfa2024p0351

Machine Learning for predicting DataCube Atomic Force Microscope (AFM): MultiDAT-AFM

COQ GERMANICUS Rosine
NORMANDIE UNIV, ENSICAEN, UNICAEN, CNRS, CRISMAT, 14000 Caen, France
rosine.germanicus@unicaen.fr

EL-HASSANI Othman
NORMANDIE UNIV, ENSICAEN, UNICAEN, CNRS, CRISMAT, 14000 Caen, France
othman.el-hassani@etu.univ-orleans.fr

Abstract

In nanoscience, techniques based on Atomic Force Microscope (AFM) stand as a cornerstone for exploring local electrical, electrochemical and magnetic properties of microelectronic devices at the nanoscale. As AFM's capabilities evolve, so do the challenges of data analysis. With the aim of developing a prediction model for AFM mappings, based on Machine Learning, this work presents a step towards the analysis and benefit of Big Data recorded in the hyperspectral modes: AFM DataCube. The MultiDAT-AFM solution is an advanced 2000-line Python-based tool designed to tackle the complexities of multi-dimensional measurements and analysis. MultiDAT-AFM offers visualization options, from acquired curves to scanned mappings, animated mappings as movies, and a real 3D-cube representation for the hyperspectral DataCube modes. In addition, MultiDAT-AFM incorporates a Machine Learning algorithm to predict mappings of local properties. After evaluating two supervised Machine Learning algorithms (out of the eight tested) for regression, the Random Forest Regressor model emerged as the best performer. With the refinement step, a root mean square error (RMSE) of 0.18, an R^2 value of 0.90 and an execution time of a few minutes were determined. Developed for all AFM DataCube modes, the strategy and demonstration of MultiDAT-AFM are outlined in this article for a silicon integrated microelectronic device dedicated to RF applications and analyzed by DataCube Scanning Spreading Resistance (DCUBE-SSRM).

Introduction

Today, the Atomic Force Microscope (AFM) offers the possibility of multidimensional measurements in several modes: electrical [1], [2], [3], infrared [4] and electrochemical [5]. In addition to the imaging part of the AFM at each pixel, spectral data set can be recorded as function of a variable. The local measurements are subjected to the impact of parameter variable on the active tip-sample nano-system, and generate a hyperspectral dataset. These techniques provide fully characterization of materials and devices, at the nanoscale. Traditional analysis tools are limited in their ability to fully process and analyze the resulting relatively large files, up to several Giga Bits with large datasets. Thus arose the need for a graphical interface capable of comprehensively analyzing, processing, visualizing and predicting these complex data sets.

With the aim of developing an AFM mappings prediction model, this work presents a step towards on the analysis and use of the Big Data recorded during AFM DataCube. To determine the best model, two Machine Learning (ML) algorithms are selected, trained and evaluated. In a microelectronic failure analysis scope, the predictive solution is proposed to help users get a better understanding of the local properties of the materials. Presented as an interface, the MultiDAT-AFM integrates many useful analysis tools and the golden ML solution with refinement, for the DataCube modes, complementary to the software supplied with AFM machines. It will empower researchers to delve deep into their data, uncovering insights previously obscured by limitations in visualization tools. As a click and show interface, Big Data analysis and predictive Machine Leaning algorithm are integrated in the MultiDAT-AFM solution. Then, the need arose for a GUI capable of reading, treating, visualizing and predicting these intricate datasets comprehensively.

Developed for all AFM electrical modes, to present the MultiDAT-AFM capabilities, this paper focus on the Scanning Spreading Resistance Microscopy (SSRM) [6], [7] in DataCube mode. Based on a case study, in a first part, the studied silicon microelectronic device and the SSRM technique are presented. The strategy and methodology of the MultiDAT-AFM solution for analysis and Machine Learning prediction is detailed in the second part. And the evaluation of mapping generation of the ML is deployed for the RF Si integrated microelectronic device.

AFM multidimensional data set: the DataCube approach

In order to record full local properties, the DataCube approach combines topography, nanomechanical properties and spectral acquisition at each pixel of the scanned area. At each pixel of the scanned area, the force curve is recorded, providing local mechanical properties. During this force curve, the AFM tip remains in contact with the surface, and during this time, known as the dwell segment, a spectral measurement of the parameters is performed and recorded as a function of the measurement variable (Figure 1).

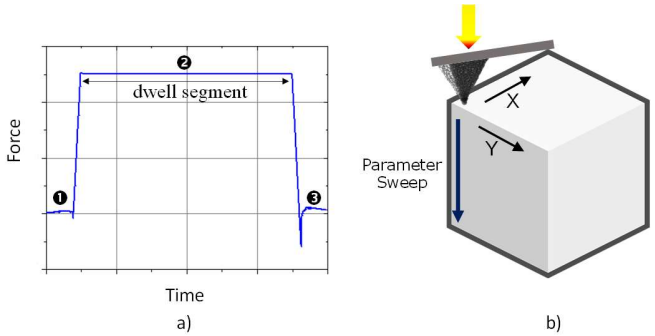

Figure 1: a) Force curve during the DataCube mode, 1: approach, 2: dwell segment and 3: tip retract, and b) schematic of the 3D DataCube hyperspectral mode with 2D topography and spectral acquisition.

TABLE I
LIST OF AFM HYPERSPECTRAL DATACUBE MODES

Name	AFM-MODE	PROBED PROPERTIES	REF for the mode
DCUBE-EFM	Electric Force Microscopy	Electric field gradient distribution	[8]
DCUBE-TUNA	Tunneling AFM	Ultra-low currents (<1pA) with high current sensitivity	[1]
DCUBE-CAFM	Conductive AFM	Currents in the 2pA to 1µA range	[9]
DCUBE-SSRM	Scanning Spreading Resistance Microscopy	Local resistance from 10^3 to 10^{12} Ω	[6]
DCUBE-SCM	Scanning Capacitance Microscopy	δC/δV signal in phase and amplitude (type and doping level)	[6]
DCUBE-sMIM	Scanning Microwave Impedance Microscopy	RF electrodynamic: permittivity and conductivity variations	[10]
DCUBE-PFM Or SSPFM	Piezoresponse Force Microscopy Switching Spectroscopy Piezoresponse Force Microscopy	electromechanical of piezoresponse	[11] [12]
DCUBE-CR	Contact Resonance	Mechanical elastic and viscoelastic	
DCUBE-SECM	Scanning electrochemical microscopy	Electrochemical	[5]

This Big Data hyperspectral modes, called DataCube or Switching Spectroscopy Mode, are used to probe mechanical, electrical, electromechanical and electrochemical properties. Table 1 lists the different DataCube modes based on AFM. For each mode, corresponding probed properties are reported and available references to illustrate the AFM mode.

For these hyperspectral modes, the sweep parameter can be a DC voltage or a frequency of the AC stimulation voltage. These modes can be very useful for failure analysis applications, when comparing a failed sample with a sample in good condition [13]. But analyzing the acquired data sets can be tedious and time-consuming for researchers and engineers.

SSRM mode and the microelectronic sample

AFM SSRM mode is a local conductive method. In this mode, the AFM conductive tip is in contact with the analyzed materials and forms a local nano-contact with the surface. As a function of the nature of the material, the electrical behavior of the nano-contact is ohmic, semi-ohmic, insulating or nano- Schottky (in the case of a semiconductor under the apex tip). At each pixel, SSRM acquires measurements of the local resistance R by a log-amplifier, with a large broad resistance range (Figure 2). The measured local resistance consists of the contribution of the probe resistance (R_{probe}) in series with sample resistance (R_{sample}) and back contact resistance with the AFM Chuck (R_{back}) [14]. For the same tip and sample, R_{probe} and R_{back} are constants. In hyperspectral DCUBE-SSRM, during the hold-segment, an DC voltage between the AFM tip and sample is applied and varied. As the DC bias is swept, the voltage dependent properties are collected.

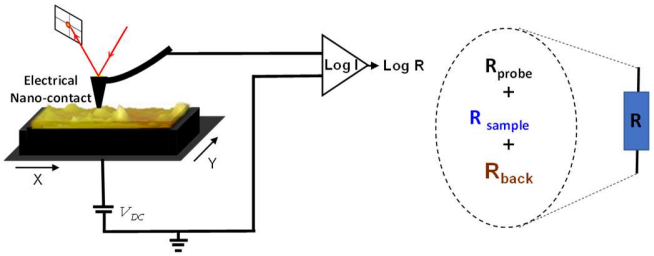

Figure 2: Schema of the SSRM mode, the local measured resistance consists of the probe resistance in series with sample resistance and back contact resistance with the AFM Chuck.

To demonstrate the capabilities of MultiDAT-AFM, an integrated silicon microelectronic device dedicated for RF applications is selected. The device consists of a highly resistive Si substrate with Deep Trench Isolation (DTI) structure. Highly resistive substrate and DTIs are used to isolate devices on the same chip and ensure good isolation for RF co-design. DTI are holes in the third direction of the silicon substrate filled with polysilicon. The device also has two level metal layers on the top of the silicon active area for electrical contact.

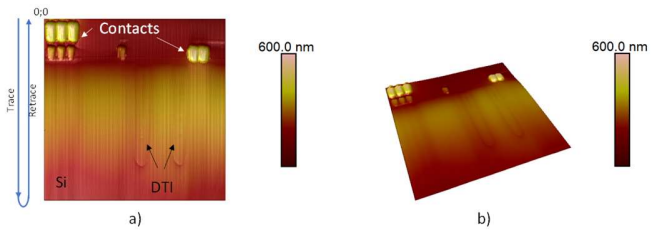

Figure 3: Topography of the studied device (cross-sectional preparation) a) 2D and b)3D view.

Sample is prepared by cross-sectional method. On the cross-section, the scanned size area is 15 µm ×15 µm with a resolution of 256 ×256 pixels. The topography is represented in Figure 3. Measurements are performed at ambient air. A high force around 10 µN was necessary on the cantilever to obtain the electrical contact with the occurrence of the β–tin zone when the tip scans silicon semiconductor [14]. Surface scratch lines can be seen on the topography measurement. Note that this property can also be used for SSRM tomography [15], [16].

Analysis tools of MultiDAT-AFM

A solution in Python is developed to treat and process the acquired data: MultiDAT-AFM, incorporating advanced visualization aspects as well as an evaluated and tested Machine Learning solution.

The solution is presented as an interface "click and show". MultiDAT-AFM offers visualization options, from acquired curves to scanned mappings, animated mappings as movies, and a real 3D-cube representation. MultiDAT-AFM doesn't require a computer with high-end specifications, and even when processing large amounts of data, it has fast execution times.

As presented, in DataCube modes, at each pixel, the approach-retract curve is recorded. The Figure 4a represents 2000 curves from the 65536 recorded (the 2000 positions are distributed over the surface) for the Si device. A zoom of the adhesion signal during the retracted step is shown. The difference of adhesions attests to the measurements of different materials with several mechanical properties. During the dwell segment (0.4 s), when the tip stays in contact, a sweep of V_{DC} from -4 V to 4 V is applied. 2000 extracted curves of log(R) as a function of the time (i.e V_{DC}) are reported on Figure 4b.

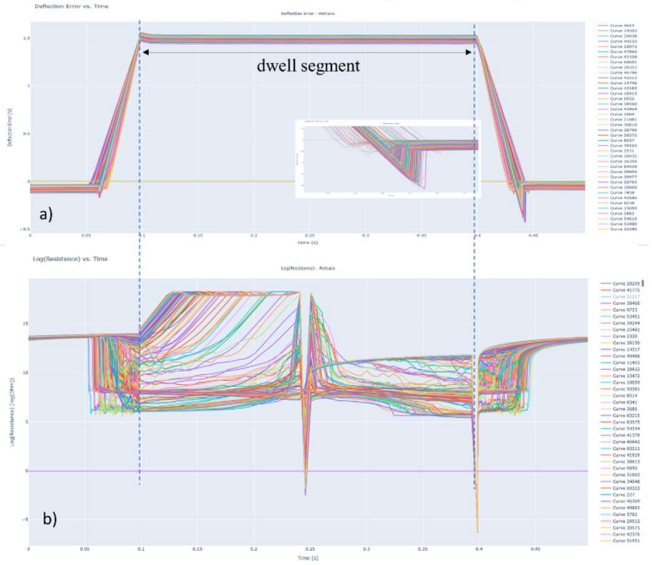

Figure 4: a) Approach-retract curves during the DCUBE-SSRM, zoom on the adhesion signal and b) raw data of log(R) recorded in SSRM as a function of the time, when a sweep is applied V_{DC} curves (from -4 V to 4 V at 0.5 Hz).

The MultiDAT-AFM solution integrates visualizations tools for the 3D-view generation as a cube (Figure 5), and ability to create animated mapping as movie from the measurement. These two tools have a very fast execution time (<1 min) and enable a clear visualization and understanding of property transitions when the measurement parameter, here V_{DC} varies.

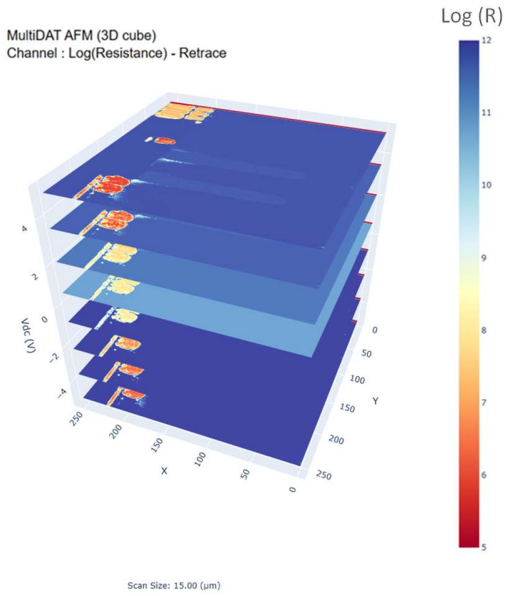

Figure 5: 3D visualization from MultiDAT-AFM of the SSRM slices at different V_{DC}

From the hyperspectral DCUBE-SSRM for each pixel local spectral Log (R) = f(V_{DC}) is recorded. Post-processing of the raw data is performed to remove outliers of the measurement technique. Secondly, the measured data are analyzed to distinguish several groups of local electrical responses related to the material properties.

In our case, to highlight the different electrical behaviors observed during SSRM measurement, Figure 6 represents the DCUBE-SSRM post-analysis. Figure 6a shows the SSRM map, slice generated for V_{DC} = 3.8 V; this value is chosen because, in this case it allows all the materials used to manufacture the component to be clearly identified. In Figure 6b two profiles along the X axis are plotted, and indicate the response levels of contact in the oxide area (top trace) and in the silicon substrate area (bottom trace). From the SSRM spectrums, I-V curves are generated. Moreover, five representative individual I-V spectral data are drawn in Figure 6c, 6d, 6e and 6f. Figure 6c, 6d, 6e for three contacts indicated by ◆■▲, respectively. And responses of the highly resistive substrate and DTI are reported in Figure 6f * and▲. This analysis shows the strength of the DataCube by highlighting the different electrical behavior. This result demonstrates the power of investigating broadband voltages compared to the typical single electrical map recorded at a single applied V_{DC}.

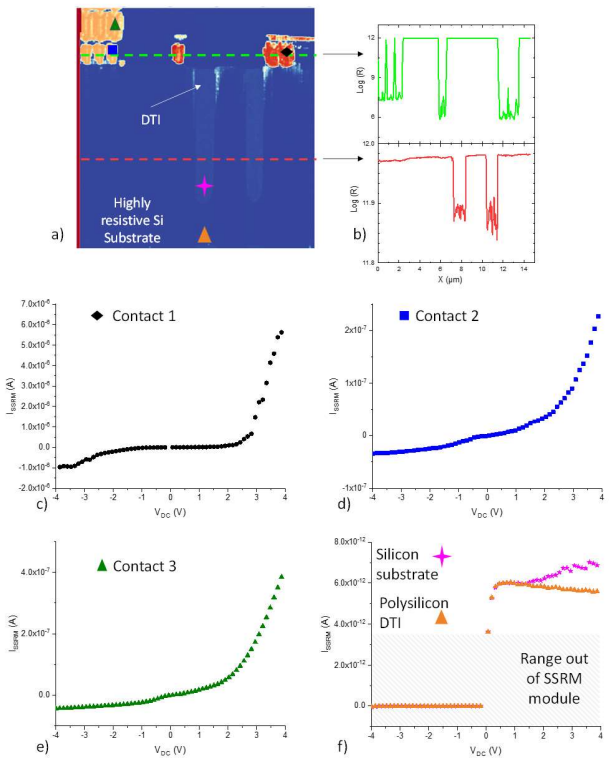

Figure 6: a) SSRM Map at V_{DC} = 3.8 V, b) resistance profiles along X axis for 2 areas, from c) to f) I-V curves generated from the SSRM measurements at 5 locations reported on the map.

Supervised Machine Learning predictive solution

From this Big Data hyperspectral result an artificial intelligence method has been investigated to take the analysis a step further. Nowadays, in AFM, Machine Learning (ML) solutions have been studied for tip evaluation, imaging classification and artifact detection, mainly from the topography and mechanical scans (in classical mode) [17]. Some publications demonstrating Machine Learning have been published for polymer blends [18] and biological cells [19], [20]. In the special case of PFM, in [12] a method is presented for analysis and data processing with Machine Learning. A Machine Learning model for the calibration of the SSRM mode is also proposed in [21]. To go further, in this paper, strategy supervised Machine Learning is employed to generate properties mappings from the database acquired during DataCube measurements. The goal is to predict the AFM value of a dependent variable based on the input. In our case, the local resistance as a function of the applied DC voltage. For the evaluation and determination of the golden model, two supervised regression models were selected on height algorithms tested. The procedure is a classical ML one, it starts with data preparation, model training and culminating in the assessment of the model's performance. The two models are applied to a calibration sample. This sample, called staircase silicon sample, consists on several P and N silicon doping area.

To evaluate the model performances two factors were mainly considered, Mean Squared Error (MSE) and Root mean squared error R^2 (RMSE) score metrics. The factors were evaluated based on: 80% training dataset and the remaining 20% for testing. Subsequently, the model is trained using 80% of the data, and it then proceeds to predict the remaining 20%. Its self-evaluation involves quantifying the degree to which its predictions deviate from the actual values, effectively gauging the accuracy of its predictive capabilities. The two models are: Gradient Boosting Regressor (GBR) and Random Forest Regressor (RFR).

Gradient Boosting Regressor (GBR) model is a popular Machine Learning algorithm used for regression issues. This solution combines multiple weak models to create a strong predictive model. The model iteratively trains decision trees to correct the errors made by the previous tree, resulting in improved accuracy. GBR is known for its speed, flexibility, and ability to handle complex data sets. The algorithm contains 3 parameters:

* n_estimators: number of decision trees, higher number of trees means higher cost of calculation
* learning_rate: the step-size or shrinkage rate used in each iteration of gradient descent. A higher learning rate can lead to faster convergence but may also cause overshooting, in this case learning_rate: = 0.1
* max_depth: the maximum depth of each decision tree. Increasing the maximum depth can improve the model's performance but may also increase the risk of overfitting.

Two n_estimators were evaluated, 10 and 100.

Random Forest Regressor (RFR) model was first proposed as a non-parametric machine-learning algorithm by Leo Breiman (Breiman 2001) [22]. Nowadays, widely used, RFR uses decision trees and ensemble learning to predict continuous outcomes. In a Random Forest Regressor, multiple decision trees are trained on random subsets of the training data. Each decision tree is built by recursively splitting the data into smaller subsets based on the best split at each node. The final prediction is made by aggregating the predictions of all the decision trees.

To evaluate the predictive performance of the models, ML predicted values versus measured (actual) DCUBE-SSRM values are compared. Results, as scatter plots, are reported in Figure 7, for the two models. The ML predicted log (R) values are plotted as a function of the measured (actual) values. From these curves Mean Squared Errors (MSE) (the average squared difference between the estimated values and the actual value) are estimated. Results with GBR with 10 trees indicates that the model is not adapted to the prediction. With 100 trees, GBR has an R-squared value of 0.8151. The Random Forest has an MSE of 0.2334, which is slightly higher than the GBR with 100 trees. The Random Forest has an R-squared value of 0.8756. This is quite high and suggests that the model is adapted to the prediction. This model serves as our "Golden Model". To improve the fitting power, the RFR is refined [23] for training and prediction purposes. For this, number of trees and nodes are optimized for the best performances and minimizing execution time. The Random Forest Regressor with refinement model emerged as the top performer among the models tested, with a

Mean Squared Error (MSE) of 0.18, R-squared value of 0.90, and an execution time of 1.26 minutes, indicating it explains about 90.06% of the variance in the data. This ML RFR refined (RFR-R) solution is then embedded to the software MultiDAT-AFM. The prediction function is divided into 3 parts: (1) Train Model, (2) Load Model and (3) Predict Maps.

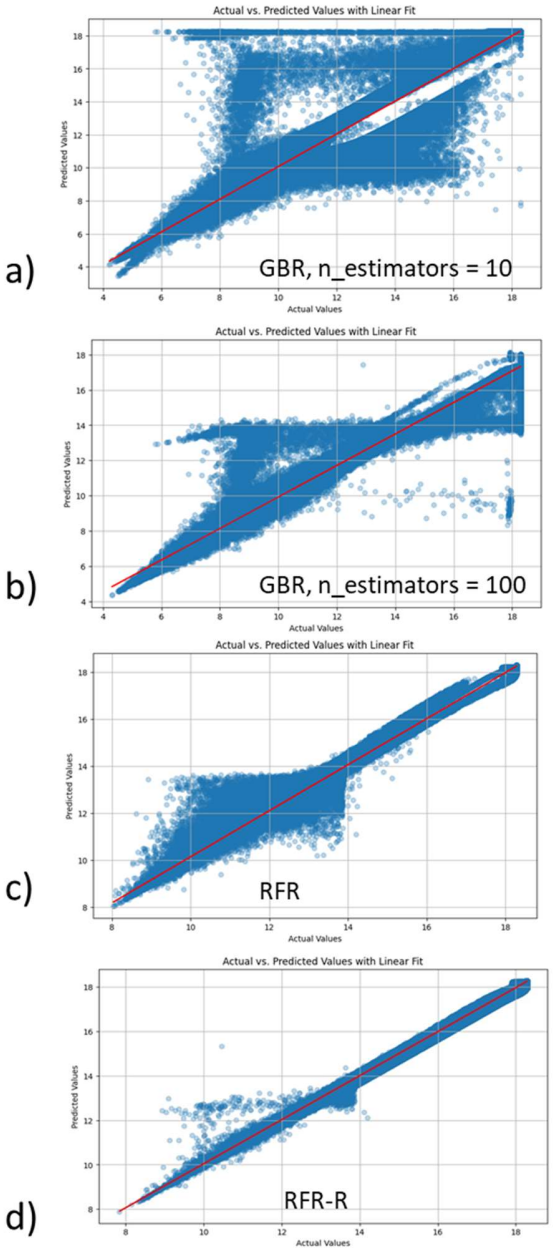

Figure 7: Scatter plots ML predicted values versus measured (actual) values of log (R) for Gradient Boosting Regressor (GBR) and Random Forest Regressor (RFR) strategies before and after Refinement (RFR-R). A linear regression line shows the trend line of the 4 scatter plot result sets.

Performances, in terms of MSE, R^2 (value near 1 is better) and execution time, on the two models with refinement are done in Table 2.

TABLE 2
EVALUATION OF THE ML MODEL

MODEL	MEAN SQUARED ERROR (MSE)	ROOT MEAN SQUARED ERROR R^2 (RMSE)	Min (s)
GBR-10	0.2303	Not a Number	181
GBR-100	0.66	0.66	16
RFR	0.2334	0.8756	2.31
RFR-R	0.18	0.90	1.26

The mapping of the errors between the measured values and predicted ones are compared before and after refinement of the RFR model on Figure 8. This evaluation step validates the RFR-R model for MultiDAT-AFM. It's important to note that at this step the ML solution is impossible to describe good and wrong measurements, as prediction is based on learning, at the bottom of the acquisition, a noisy response can also be predicted.

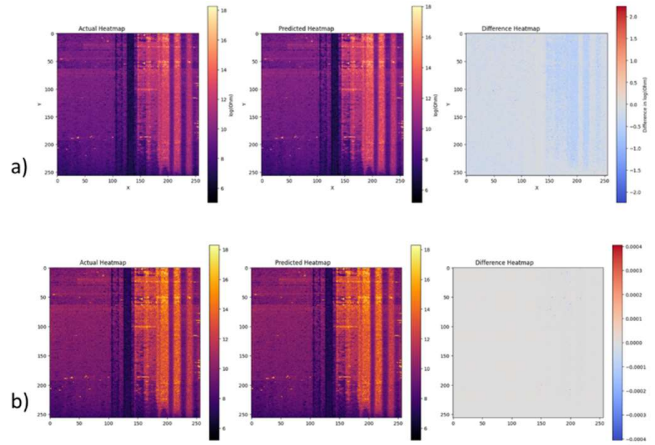

Figure 8: Predictive model by Random Forest Regressor model integrated in MultiDAT-AFM, a) before and b) after refinement. The sample is a staircase one, a calibration sample with several silicon doped layers: measured, predictive and error mappings of log (R).

For the studied integrated RF microelectronic device using a highly resistive silicon substrate, four mappings predicted are drawn in Figure 9, at four V_{DC} (related at time in the tool). Comparison of actual and predicting mappings demonstrate the capabilities of MultiDAT-AFM solution on known good samples. These results open new opportunities. In fact, the generation of predicted maps, inside the V_{DC} range measurements, can reduce the relative long DataCube's acquisition time, by reducing the number of measurements on the desired V_{DC} range and supplementing it with maps predicted by MultiDAT-AFM. This would also counteract any change in surface during measurement.

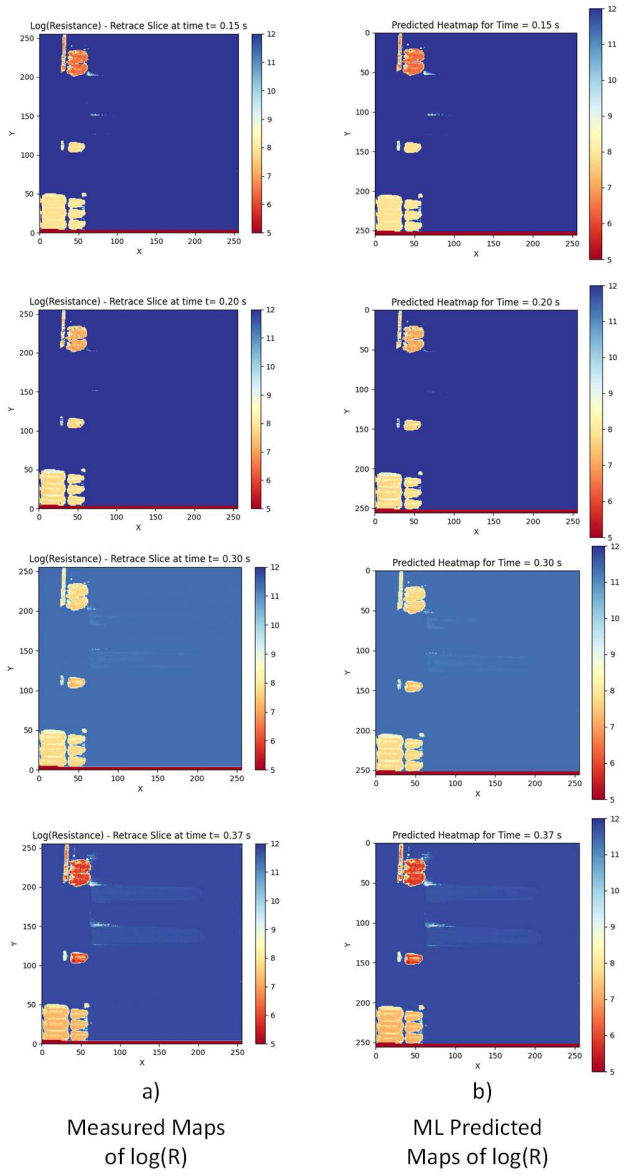

Figure 9: MultiDAT-AFM prediction of mappings, compared with measured mappings for different applied V_{DC} (related to the time).

Conclusions

MultiDAT-AFM is a tool for analyzing and predicting matches from DataCube. With this solution, visualizations tools are embedded in order to examine with the utmost precision datasets from the AFM DataCube modes. Post-measurement analysis is possible to highlight complete differences in the AFM probed electrical behavior. The Random Forest Regressor model with refinement (RFR-R) provides successful results for the DCUBE-SSRM. Tests are also performed for DC-SCM with the same performances. For the further, the medium-term goal is to cover multiple samples and including different DataCube modes. MultiDAT-AFM can help experts in microelectronic failure analysis to better elucidate degradation mechanisms at the microelectronic chip level. The question of predicting maps beyond the measurement range is also raised and need testing and validation investigations. To move towards clustering and classification can be after used for material recognition from the experimental DataCube datasets. This applying step must be adapted to each type of component studied, since it is closely linked to the nature of the materials used.

Acknowledgments

The authors also would like to thank CARNOT ESP Institute for supporting the SiCAgeing research project.

References

[1] P. D. Wolf *et al.*, “Functional Imaging with Higher-Dimensional Electrical Data Sets,” *Microscopy Today*, vol. 26, no. 6, pp. 18–27, Nov. 2018, doi: 10.1017/S1551929518001025.

[2] P. De Wolf, Z. Huang, and B. Pittenger, “Spectroscopy-Based Mapping with Scanning Microwave Impedance Microscopy,” presented at the ISTFA 2018, ASM International, Nov. 2018, pp. 550–554. doi: 10.31399/asm.cp.istfa2018p0550.

[3] R. C. Germanicus *et al.*, “Mapping of integrated PIN diodes with a 3D architecture by scanning microwave impedance microscopy and dynamic spectroscopy,” *Beilstein J. Nanotechnol.*, vol. 11, no. 1, pp. 1764–1775, Nov. 2020, doi: 10.3762/bjnano.11.159.

[4] A. M. Charrier, A. C. Normand, A. Passian, P. Schaefer, and A. L. Lereu, “In situ plant materials hyperspectral imaging by multimodal scattering near-field optical microscopy,” *Commun Mater*, vol. 2, no. 1, pp. 1–12, Jun. 2021, doi: 10.1038/s43246-021-00166-7.

[5] X. Shi, W. Qing, T. Marhaba, and W. Zhang, “Atomic force microscopy - Scanning electrochemical microscopy (AFM-SECM) for nanoscale topographical and electrochemical characterization: Principles, applications and perspectives,” *Electrochimica Acta*, vol. 332, p. 135472, Feb. 2020, doi: 10.1016/j.electacta.2019.135472.

[6] R. Coq Germanicus and U. Lüders, “Electrical Characterizations Based on AFM: SCM and SSRM Measurements with a Multidimensional Approach,” *EDFA Technical Articles*, vol. 24, no. 3, pp. 24–31, Aug. 2022, doi: 10.31399/asm.edfa.2022-3.p024.

[7] R. Elpelt, B. Zippelius, S. Doering, and U. Winkler, “Employing Scanning Spreading Resistance Microscopy (SSRM) for Improving TCAD Simulation Accuracy of Silicon Carbide,” *Materials Science Forum*, vol. 897, pp. 295–298, 2017, doi: 10.4028/www.scientific.net/MSF.897.295.

[8] P. Girard, “Electrostatic force microscopy: principles and some applications to semiconductors,” *Nanotechnology*, vol. 12, no. 4, p. 485, Nov. 2001, doi: 10.1088/0957-4484/12/4/321.
[9] C. Zhang and E. P. Y. Chen, “Conductive-AFM for Failure Analysis of Parametric Test Structures in Advanced Technology Development,” presented at the ISTFA 2017, ASM International, Nov. 2017, pp. 143–147. doi: 10.31399/asm.cp.istfa2017p0143.
[10] R. C. Chintala, N. Antoniou, and Y. Yang, “Advances in Scanning Microwave Impedance Microscopy,” presented at the ISTFA 2021, ASM International, Oct. 2021, pp. 436–440. doi: 10.31399/asm.cp.istfa2021p0436.
[11] A. Cui *et al.*, “Probing electromechanical behaviors by datacube piezoresponse force microscopy in ambient and aqueous environments,” *Nanotechnology*, vol. 30, no. 23, p. 235701, Mar. 2019, doi: 10.1088/1361-6528/ab0866.
[12] H. Valloire, P. Quéméré, N. Vaxelaire, H. Kuentz, G. Le Rhun, and Ł. Borowik, “Enhancing ferroelectric characterization at nanoscale: A comprehensive approach for data processing in spectroscopic piezoresponse force microscopy,” *Journal of Applied Physics*, vol. 135, no. 19, p. 194101, May 2024, doi: 10.1063/5.0197226.
[13] P. De Wolf, “Review of Scanning Probe Microscopy Methods for Failure Analysis (2023 Update),” presented at the ISTFA 2023, ASM International, Nov. 2023, pp. i1–i45. doi: 10.31399/asm.cp.istfa2023tpi1.
[14] R. Coq Germanicus *et al.*, “On the effects of a pressure induced amorphous silicon layer on consecutive spreading resistance microscopy scans of doped silicon,” *Journal of Applied Physics*, vol. 117, no. 24, p. 244306, Jun. 2015, doi: 10.1063/1.4923052.
[15] C. Noël, L. Wouters, K. Paredis, U. Celano, and T. Hantschel, “Oil as an Enabler for Efficient Materials Removal in Three-Dimensional Scanning Probe Microscopy Applications,” *Front. Mech. Eng.*, vol. 7, Dec. 2021, doi: 10.3389/fmech.2021.797962.
[16] R. C. Germanicus *et al.*, “Three dimensional resistance mapping of self-organized Sr3V2O8 nanorods on metallic perovskite SrVO3 matrix,” *Applied Surface Science*, vol. 510, p. 145522, Apr. 2020, doi: 10.1016/j.apsusc.2020.145522.
[17] M. A. Rahman Laskar and U. Celano, “Scanning probe microscopy in the age of machine learning,” *APL Machine Learning*, vol. 1, no. 4, p. 041501, Nov. 2023, doi: 10.1063/5.0160568.
[18] D. Yablon, I. Chakraborty, J. Thornton, and B. Pittenger, “Machine Learning to classify, predict structure-property relationships, and detect artifacts in AFM images,” vol. 2023, p. M36.002, Jan. 2023.
[19] I. Sokolov, “On machine learning analysis of atomic force microscopy images for image classification, sample surface recognition,” *Physical Chemistry Chemical Physics*, vol. 26, no. 15, pp. 11263–11270, 2024, doi: 10.1039/D3CP05673B.
[20] Y. Zeng, X. Liu, Z. Wang, W. Gao, L. Li, and S. Zhang, “Detection and classification of hepatocytes and hepatoma cells using atomic force microscopy and machine learning algorithms,” *Microscopy Research and Technique*, vol. 86, no. 8, pp. 1047–1056, 2023, doi: 10.1002/jemt.24384.
[21] L. Wouters, “On the Impact of Artificial Intelligence in Electrical Modes for Atomic Force Microscopies,” presented at the ISTFA 2023, ASM International, Nov. 2023, pp. p1–p65. doi: 10.31399/asm.cp.istfa2023tpp1.
[22] L. Breiman, “Random Forests,” *Machine Learning*, vol. 45, no. 1, pp. 5–32, Oct. 2001, doi: 10.1023/A:1010933404324.
[23] S. Ren, X. Cao, Y. Wei, and J. Sun, “Global refinement of random forest,” in *2015 IEEE Conference on Computer Vision and Pattern Recognition (CVPR)*, Jun. 2015, pp. 723–730. doi: 10.1109/CVPR.2015.7298672.